Synthesis, Characterization, and Application of Noble Metal and Noble Metal Alloy Nanoparticles to Proton Exchange Membrane Fuel Cells for Enhanced Catalytic Activity

Xiaotian Zhang[1] and Arun Soni[1]
[1] Staples High School. 70 North Ave. Westport, CT 06880 USA

24 September, 2015

Abstract

Nanoparticles can be engineered with unique compositions, shapes, and sizes. Because of this flexibility, they are used in a growing list of applications in science and industry.[1] Using a modified two-phase Brust-Schiffrin method, we synthesized noble metal nanoparticles and alloy nanoparticles including Au, AuAg, AuPt, Ag, PtAg, Pt, AuPt 1:6, AuPt 6:1, AuPt 1:3, and AuPt 3:1.[2] We then characterized them using Transmission Electron Microscopy, UV-Visible Spectroscopy, and Zeta Potential analysis techniques. Most particles were between 2 and 6 nm in diameter, with the exception of Ag which had a mean diameter of 27 nm. 200 μL of nanoparticle suspension were coated onto 5 by 5 cm Nafion 117 membranes used in Proton Exchange Membrane Fuel Cells (PEMFC) to test for catalytic activity. Contrary to previous literature that reported AuPt as the best coating for improving catalytic efficiency, we found that the AuAg coating was more effective.[3] At maximum output, the AuAg-coated PEMFC resulted in 73% more power output compared to the control PEMFC and 10% more compared to the AuPt-coated PEMFC.[4] AuAg particles showed significantly greater stability in suspension than did AuPt with a high Zeta Potential of -84.66 mV, which suggests long shelf life. We demonstrate an environmentally and economically feasible process to improve PEMFC using AuAg nanoparticles.

1 Introduction

Fossil fuels pollute the environment and will eventually be unsustainable to use for energy production in a number of cases, notably in automobiles.[5] Various companies have experimented with hydrogen fuel cells as an alternative source of energy, but there is still much room for improvement to increase the efficiency of these cells. We hypothesize that using noble metal nanoparticles to coat proton exchange membranes (PEM) can alter the efficiency of PEM fuel cells, and have synthesized a variety of nanoparticles to achieve the goal of maximum efficiency enhancement.

1.1 Why Noble Metal Nanoparticles?

Platinum is a good catalyst for reactions required in the PEM fuel cell, such as $H_2 + \frac{1}{2}O_2 \longrightarrow H_2O$ and $CO \longrightarrow CO_2$.[6] We believed that turning platinum into a nanoparticle would enhance hydrogen gas catalysis, but platinum has two primary drawbacks: it is expensive and is easily poisoned by carbon monoxide, which drastically decreases the efficiency of the cell. Gold nanoparticles were selected for their ability to catalyze the $CO \longrightarrow CO_2$ reaction, fundamental for preventing CO poisoning, but also have a high overall cost.[7] Silver was chosen as a third noble metal because it is highly reactive and cost-effective but is oxidized easily, which leads to instability.[8] Alloys between two of the three were made in an attempt to combine their positive properties and neutralize their negative effects.

Gold has been regarded as catalytically inert due to its stability; however, it has been discovered to be 1000 times more active than Pt in the electrochemical and catalytic oxidation of CO in basic environments.[9] Haruta, Yates et al., and others have demonstrated the effectiveness of Au nanoparticles as a catalyst of the CO oxidation reaction.[9,10] Haruta describes the catalysis as a gold-substrate synergy that allows very low activation energies to catalyze $CO \longrightarrow CO_2$, even at low temperatures. However, the high temperatures that he utilized for formation and deposition of the particles on TiO_2 are not practical for polymer membrane applications. Because the CO oxidation enhancement reported on TiO_2 occurred when the

gold nanoparticles were in a single layer, we coated nanoparticles onto the PEM (Nafion 117) surface using a Langmuir-Blodgett trough.[9]

Yates et al. and Neurock et al. explained gold's enhanced CO oxidation by proposing that Au nanoparticles formed a step-like structure on the TiO_2 substrate.[11,12] This structure enabled a two-step oxidation process to occur along the reactant sites, causing C≡O bond-stretching and consequently more CO to form CO_2, which led to a decrease in CO poisoning for platinum, an increase in fuel cell efficiency, and a decrease in necessary operating temperature.[11,12] Adzic et al. proposed a core-shell structure with Pt as the core and Pd as the shell to protect the platinum from poisoning.[6] We propose that such a structure can occur with other noble metal alloys, and will significantly improve the power output of the system.

1.2 Why Proton Exchange Membrane Fuel Cells?

Proton Exchange Membrane Fuel Cells (PEMFC) works as shown in Figure 1. The hydrogen gas pumped in through the anode side is split into H^+ ions and electrons by the catalyst. Electrons flow through the anode-cathode connection. On the cathode side, the H^+ and electrons are combined with oxygen from the air to form H_2O for a clean conclusion to the energy generation process.

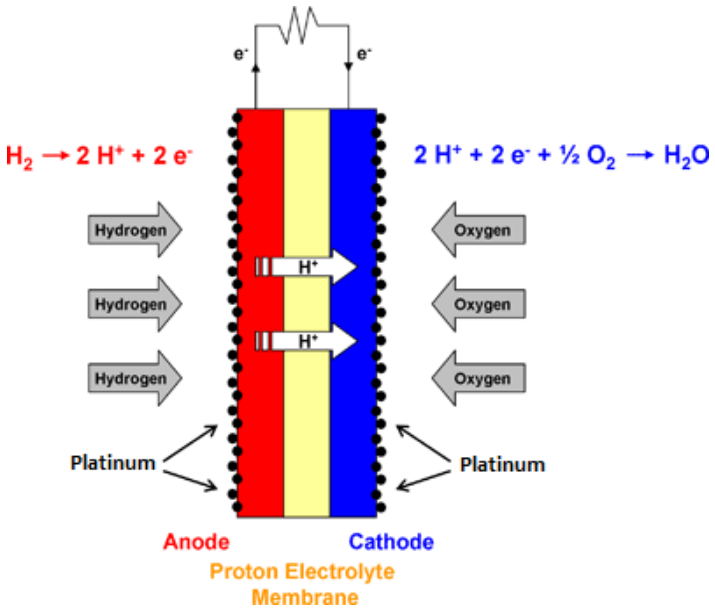

Figure 1: A diagram of a functioning PEMFC, with the PEM (Nafion 117) in between the two electrodes (carbon paper with platinum catalyst manufactured by Fuel Cells Etc).[15]

PEMFC were chosen to study for various reasons. In the past, PEMFC have been used in spacecraft but have been avoided in ground transportation due to high operating costs.[13] In recent years, they have become more economically feasible due to improvement in thin film manufacturing and platinum catalyst application.[14] The solid yet flexible electrolyte membrane does not leak or crack, and the lightweight cells can operate at a low enough temperature to make them practical for cars and homes.[14] The high operating temperatures of other fuel cells would be incompatible with our nanoparticles and could be potentially dangerous, since toluene was involved in the synthesis process.

1.3 Objectives

The objectives of this work are listed as follows:

1. Synthesize noble metal nanoparticles and alloy nanoparticles of varying ratios
2. Characterize synthesized noble metal nanoparticles
3. Apply nanoparticles to Nafion 117 membranes and test the PEMFC to determine the optimal combination of noble metals for catalytic activity

2 Methods and Materials

2.1 Synthesis of Noble Metal Nanoparticles

We used a two-phase modified Brust-Schiffrin method for the synthesis of pure metallic and bimetallic nanoparticles.[2] First, 656 mg of TOABr (Tetraoctylammonium Bromide) in 24 mL of toluene was prepared for each nanoparticle sample. TOABr, a phase transfer agent, was crucial to the two-phase synthesis method: it transferred the metal from water to toluene. Then, 0.25 mmol of metal salt in 9 mL of deionized water solution was prepared. For alloys, the total mmol of metal salt was 0.25 (in a 1:1 ratio alloy, there would be 0.125 mmol of each salt). The two mixtures were poured into a round-bottom flask and stirred using a magnetic stirring bar at maximum power. While stirring, the flask was covered with aluminium foil to prevent evaporation of toluene. Toward the end of mixing, 113.5 mg of $NaBH_4$, a reducing agent, in 7.5

mL of deionized water was prepared. After 20 minutes, 200 μL of 1-dodecanethiol and then the $NaBH_4$ solution were added to the round-bottomed flask. 1-dodecanethiol was a capping agent which controlled the size of the particles by preventing coagulation. The resulting mixture was stirred for 3 hours while covered with aluminium foil that prevented evaporation. We took turns preparing ingredients, cleaning equipment, and creating mixtures to maximize productivity. A significant portion of ingredient preparation required collaboration. After stirring, the mixture was carefully transferred to a separation funnel. At this stage, the clear water-based portion was on the bottom of the flask, and the toluene-based portion appeared brown if silver or gold-based, or slightly orange if platinum-based. The water was removed first by opening the valve. One drop of toluene was allowed to escape before closing the valve to ensure that all water was removed. A test tube was filled with the remaining toluene nanoparticle suspension.

The sample was dried on a rotary evaporator under a 40°C water bath to evaporate the toluene faster than at room temperature until 5 mL of mixture remained, and then was washed with 50 mL ethanol. The suspension was centrifuged at 2500 rpm for 20 minutes, and an aspirating system was used to remove the ethanol. The ethanol washing was done twice per sample. After washing with ethanol, the sample was dried in the vacuum desiccator (a low pressure environment to increase the speed of the drying process). After 48 hours, the nanoparticles were removed by spatula and resuspended in toluene at a 1 mg/mL concentration. The nanoparticles that had a platinum component were noticeably more difficult to remove from the spatula and weighing paper than were the other nanoparticles since they adhered to both surfaces, which hints at a difference in particle behavior.

2.2 Characterization of Nanoparticles

Particles were analyzed using ultraviolet-visible spectroscopy, and the graphs were analyzed for peak wavelengths to show presence of nanoparticles and the distribution of nanoparticle sizes.

For the Zeta Potential Test, suspensions of 1 mg/mL noble metal nanoparticles in toluene were diluted 10x. The stability of the suspensions was rated according to the scale in Table

1. Our mentor taught us operating techniques for both the UV-Visible and Zeta Potential instruments, so we maximized time-efficiency by performing both tests concurrently.

Zeta potential [mV]	**Stability of colloidal dispersion**
from 0 to ±5,	Rapid coagulation or flocculation
from ±(10 to 30)	Incipient instability
from ±(30 to 40)	Moderate stability
from ±(40 to 60)	Good stability
more than ±61	Excellent stability

Table 1: Zeta Potential Test Ratings describing the stability of our nanoparticles in toluene suspension. Larger numbers correspond to higher stability due to larger electrostatic dispersion between particles.[16]

All samples were subjected to Transmission Electron Microscopy to determine the dispersion, surface topography, and mean particle size. ImageJ software was used to measure particle size.

2.3 Coating Nanoparticles on the Nafion Membrane

Using a Langmuir–Blodgett trough (LB trough), we coated 1 mg/mL Ag, Au, AuAg, PtAg, AuPt, and AuPt 6:1 in toluene on 5 cm by 5 cm Nafion 117 membranes. Our mentor pre-approved samples to be coated so that no contamination of the this key instrument would occur.

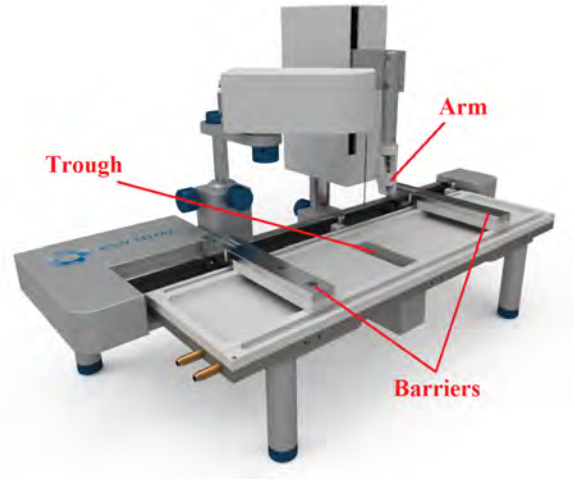

Figure 2: A computer-drawn image of a Langmuir-Blodgett trough. Notable components include the computer-controlled dipping mechanism (arm), the trough in the middle, and the two barriers that converge to the middle of the instrument during the coating process.[17]

An LB Trough is made of Teflon filled with water to create a surface and has barriers that can move across the surface. The coating process started with cleaning the trough and barriers with ethanol, filling the container with deionized water, using a vacuum to remove dust, hair, and other contaminants from the well, and then conducting a surface pressure water test to ensure quality. If the test showed surface pressures (water quality) between -0.5 mN/m to +0.5 mN/m, we proceeded to slowly drip 200 μL of nanoparticles dissolved in toluene over the surface using a Microliter Hamilton Co. syringe. If the water test failed, we would clean the surface by vacuum and try again. We waited five minutes to allow the toluene to evaporate and then moved the barriers closer, allowing water to flow under the barrier but causing hydrophobic surface molecules to remain on the surface between the two barriers. During the barrier moving process, a surface pressure/area isotherm curve was generated by monitoring surface pressure as a function of surface area. Then the entire process was repeated, but a Nafion membrane was placed in the trough for coating. The barriers moved at 8 mm/min and stopped moving at a target pressure of 3 mN/m. As the Nafion membrane was lifted with the mechanical arm of the LB Trough, it was automatically coated.

2.4 Testing Power Output

We soaked the coated polymer membrane in deionized water for 5 minutes due to its hydrophobicity, and prepared our fuel cell by adding platinum catalyst layers to both the anode and cathode side. The membrane was then placed between two platinum catalyst film layers, closing the fuel cell membrane electrode assembly (MEA) (see Figure 1 for setup of the MEA and Figure 3 for setup of the exterior system). The setup was secured using four sets of nuts and bolts. A copper tube carrying pressurized H_2 gas with flow rate of 80 cc/min and pressure of 20 psi was connected to one area of the fuel cell and another tube that carried waste out of the system was connected to a second area. The flow rate was controlled by a Supelco carboloy ball flow meter. Wires for the ammeter and voltmeter were also connected to their respective positions. We varied the *additional* resistance of the system over the following set of values: 0, 1, 2, 3, 4, 5, 6, 7, 8, 9, 10, 15, 60, 240, and ∞ Ω and recorded current and voltage over

30 second intervals for each resistance value (we are *not* short-circuiting the system at 0 Ω of added resistance, as there is still internal resistance). Each trial was repeated three times to ensure accuracy. Power was determined by multiplying the current with the voltage. We took turns recording data and timing the intervals of data collection.

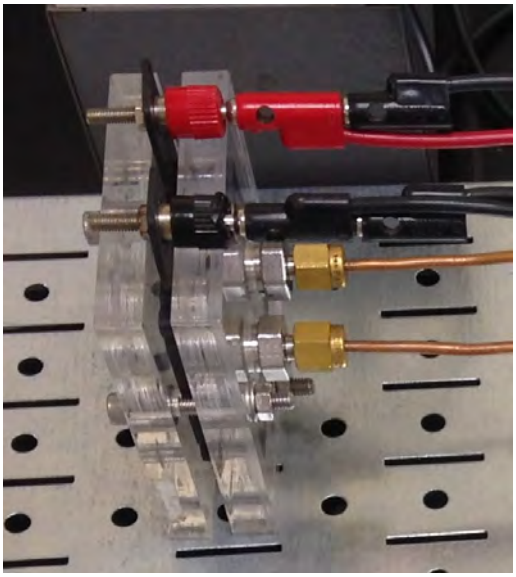

Figure 3: A setup of the fuel cell testing station. One copper tube carries H_2 gas flowing to the fuel cell, and the other carries waste generated by the system away to the fume hood. The internal components of the cell are present as diagrammed in Figure 1. Wires are connected to the voltmeter and ammeter in order to collect data.

2.5 Materials

The gold, silver, and platinum salts used in this paper include Sigma-Aldrich 99.9995% $KAuCl_4$, 99.9999% $AgNO_3$, and 99.9% K_2PtCl_4. Synthesis ingredients included Sigma-Aldrich 98% TOABr, 98.5% $NaBH_4$, 98% 1-Dodecanenthiol, and 99% toluene. Transferring 200 μL 1-dodecanethiol from the bottle required the use of an Eppendorf Micropipette. A Sigma-Aldrich single neck round bottom flask and separation funnel were used for mixing and water-toluene separation respectively. SARSTEDT Aktiengesellschaft & Co. polystyrene serological pipettes of 1, 5, 10, and 25 mL and a pipette bulb were used to transfer liquids other than toluene. When the mixing was completed, the suspension was transferred from the separation funnel to a 50 mL Polypropylene Conical Falcon Tube (resistant to toluene damage). Weighing was done on VWR Scientific Products weighing paper in an iBalance 211 scale and a UMX2

Ultra-microbalance for masses near 1 mg. The synthesis procedure was conducted in a Fisher Hamilton Safeaire Fume Hood. The Sigma-Aldrich vacuum desiccator and rotary evaporator machine were used to remove toluene and ethanol in the synthesis procedure, and the Damon Cell Division Centrifuge Machine IEC HN-S II separated ethanol and the nanoparticles. We used a custom aspirating system with a high flow rate water faucet and waste container to remove ethanol. Ethanol, detergent, and Kimtech wipes were used to clean glassware. For characterization, 5 mL VWR glass pipettes were used to transfer toluene suspensions into glass vials for the Thermo Scientific Evolution 220 UV-Visible Spectrophotometer and to dilute suspensions for the Nanobrook Omni Zeta Potential Machine. Zeiss EDX and TEM Machines were used to further characterize samples. A KSV Langmuir-Blodgett Trough was used for coating Nafion membranes. The fuel cell consisted of two electrodes (carbon paper with platinum catalyst manufactured by Fuel Cells Etc) and a 183 μm, 5 cm by 5 cm Nafion 117 membrane, which is a perfluorinated ion-exchange membrane from Sigma-Aldrich. For testing, Praxair compressed H_2 flow rate was controlled by an Analytical Supelco Bellefonte PA Flow meter with a carboloy ball. An Eico Electronic Instrument Co. Model 1171 Resistor Box controlled the resistance of the circuit. A Fluke 800A Digital Voltmeter and Keithley 195A Digital Ammeter measured the voltage and current.[4]

3 Results and Discussion

3.1 Synthesis and Characterization

After synthesis, the nanoparticles were examined in three ways: Ultraviolet-Visible Spectroscopy, Zeta Potential Analysis, and Transmission Electron Microscopy. When one member prepared samples for TEM, the other performed UV-Visible spectroscopy on the adjacent table; when one member measured and analyzed the TEM images with ImageJ, the other would look at data from UV-Visible spectroscopy and Zeta Potential tests. One person would search for literature relevant to the topic, and the other would typeset the paper, look for graphics, and perform analysis on the data.

Ultraviolet-Visible Spectroscopy

One measurement used to characterize our samples was UV-Visible Spectroscopy, which measured absorbance in the ultraviolet-visible spectral region (wavelength 300 nm to 700 nm).

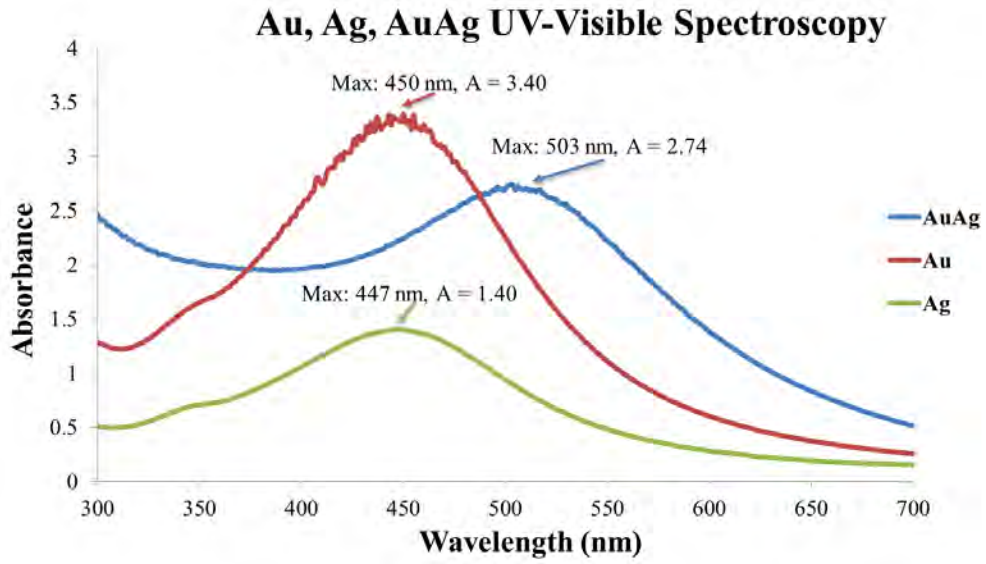

Figure 4: Wavelength vs. Absorbance curve for AuAg, Au, Ag nanoparticles determined by UV-Visible Spectroscopy. Each colloid had a characteristic peak that was compared to those found in literature.

The wavelengths at plasmonic peaks can be correlated to specific types of nanoparticles. The peak at 450 nm for Au (red arrow) confirms the presence of gold nanoparticles that are approximately 5 nm in diameter and the peak at 447 nm for Ag (green arrow) confirms the presence of silver nanoparticles.[18,19] This rightward shift for AuAg's peak (blue arrow) compared to its component's peaks was interesting and unexpected, and shows that our alloy has new properties rather than just being the average of its components. The width of the peak examined showed the standard deviation for the size of the particles. Au nanoparticles had the narrowest peak, meaning more monodispersed particles, whereas Ag nanoparticles had the broadest peak, meaning a wide distribution of particle sizes. AuAg was in between, meaning relatively consistently sized particles. This was shown by our TEM data as well. Any sample containing platinum did not show workable data due to platinum's lack of plasmonic activity. Noise from the platinum samples made the data impossible to analyze, and showed no discernible peaks.

Zeta Potential

The Zeta Potential is a key indication of the stability of a colloidal suspension. The magnitude of Zeta Potential shows the degree of electrostatic repulsion between charged particles in a suspension. A high Zeta Potential means the suspension will resist aggregation and possess high stability.

	Zeta Potential (mV)				
Particle	Ag	AuAg	Au	AuPt 6:1	AuPt
Mean	-42.60	-84.66	-32.39	-22.87	-9.35
Standard Error:	13.68	35.61	4.27	5.25	29.18

Table 2: The mean and standard error Zeta Potential (mV) measurements of various nanoparticle colloid samples, determined by the Nanobrook Omni Zeta Potential instrument.

AuAg, with a Zeta Potential of -84.66 mV, had excellent stability that shows the practicality of such a nanoparticle suspension being used in scaled-up synthesis and storage. However, nanoparticle suspensions containing even low concentrations of platinum led to low stability, with AuPt 6:1 and AuPt having Zeta Potentials of -22.87 mV and -9.35 mV, both considered as having incipient instability. This was most likely due to the 1-dodecanethiol's S−H group not being an effective capping agent to platinum, as thiols have an affinity for gold and silver, but not platinum.[20]

Transmission Electron Microscopy

With the aid of our mentor (minors were not allowed in the TEM room for safety reasons), all samples were examined under a transmission electron microscope at magnification between 30,000x and 200,000x, depending on nanoparticle size. Figure 5 is a TEM image of AuAg nanoparticles at 150,000x magnification showing relatively monodispersed, spherical, and small particles. Figure 6 is a TEM image of Ag nanoparticles at 30,000x magnification showing polydispered, large, rounded triangular and hexagonal particles.

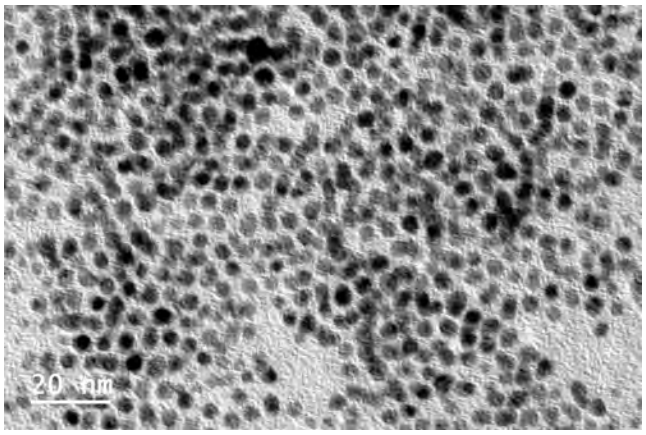

Figure 5: AuAg TEM image at 150,000x magnification (20 nm scale). Mean particle diameter was 4.21 ± 0.56 nm.

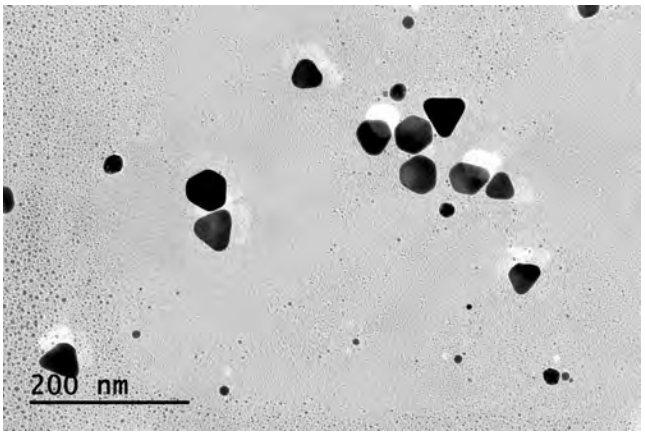

Figure 6: Ag TEM image at 30,000x magnification (200 nm scale). Mean particle diameter was 28.33 ± 8.6 nm.

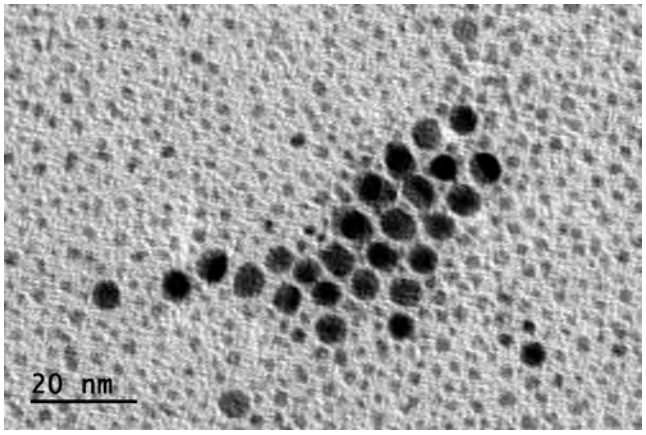

Figure 7: Au TEM image at 200,000x magnification (20 nm scale). Mean particle diameter was 5.78 ± 0.64 nm.

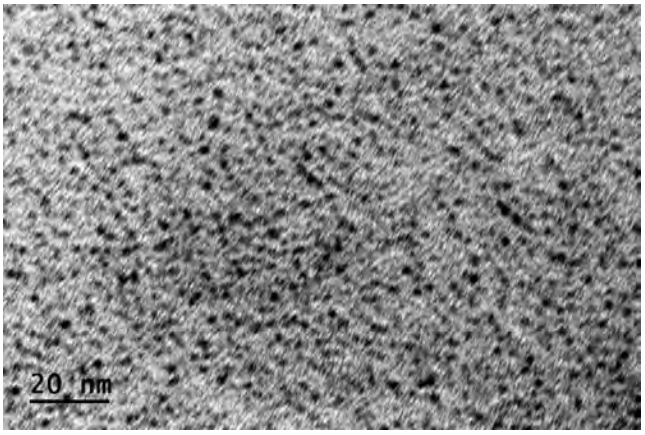

Figure 8: AuPt TEM image at 150,000x magnification (20 nm scale). Mean particle diameter was 2.39 ± 0.47 nm.

Figure 7 is a TEM image of Au nanoparticles at 200,000x magnification showing relatively polydispersed, spherical, and small particles. Figure 8 is a TEM image of AuPt nanoparticles at 150,000x magnification showing monodispersed, spherical, and small particles.

Calculations for mean particle size were determined with ImageJ software using the scale on the TEM images to find the diameter of each particle. Between 50 and 200 particles were used to determine each mean value. Table 3 shows the mean diameter and standard deviation of each particle that was synthesized.

Particle	Mean Diameter (nm)	Standard Deviation (nm)
AuPt	2.39	0.47
PtAg	2.43	0.38
AuPt 1:6	3.06	0.63
AuPt 6:1	3.41	0.60
AuAg	4.21	0.56
Pt	4.55	1.26
AuPt 1:3	4.56	0.93
AuPt 3:1	5.27	0.99
Au	5.78	0.64
Ag	28.33	8.60

Table 3: Particle size comparison for all synthesized noble metal alloy nanoparticle samples. Particles were sorted in order of increasing size for ease of comparison.

AuPt has the smallest mean size of 2.4 nm ± 0.5 nm and Ag has the largest mean size of 28.33 nm ± 8.6 nm. As discussed in the UV-Visible Spectroscopy section, there was a rightward shift in the peak of AuAg compared to both Au and Ag. This was partly due to the decrease in the mean particle size of AuAg by 1.57 nm compared to Au and 24.12 nm compared to Ag.

Surface area is a primary factor in catalytic activity. An increase in total surface area increases binding sites for reactants. In Table 4, total surface area was calculated for 200 μL of each nanoparticle suspension (the volume of each particle suspension used in the hydrogen fuel cell testing).

Particle	Mean Radius (nm)	Volume (m^3)	Density (g/cm^3)	Total Surface Area (m^2)
Ag	14.2	1.19E-23	10.5	0.0040
Au	2.9	1.01E-25	19.3	0.0108
AuPt 3:1	2.6	7.66E-26	19.8	0.0115
Pt	2.3	4.93E-26	21.5	0.0123
AuPt 1:3	2.3	4.98E-26	20.9	0.0126
AuPt 6:1	1.7	2.08E-26	19.6	0.0179
AuPt 1:6	1.5	1.50E-26	21.2	0.0185
AuAg	2.1	3.92E-26	14.9	0.0191
AuPt	1.2	7.12E-27	20.4	0.0247
PtAg	1.2	7.47E-27	16.0	0.0310

Table 4: Calculated total surface area comparison for all nanoparticle samples. We assume that the mass density of an alloy is the weighted average of the mass densities of its components.

To calculate these surface areas, we begin at the surface area of one particle, A_1. We approximate particles to be perfect spheres.

$$A_1 = 4\pi r^2 \tag{1}$$

where r is the particle's radius in meters. Then, the number of particles N in a volume V (m^3) is:

$$N = V/(C_1 \frac{4}{3}\pi r^3 \rho) \tag{2}$$

where ρ is the metal's density in g/cm^3 and C_1 is 10^6 m^3/kg. The total surface area in m^2, A_{total} is:

$$A_{total} = NA_1 = \frac{3C_1V}{\rho r} \tag{3}$$

PtAg had the highest total surface area of 0.031 m^2 and Ag had the lowest total surface area of 0.004 m^2. A notable nanoparticle is again AuAg because of a size to total surface area anomaly caused by its low density. It has a diameter nearly double that of AuPt 1:6 and AuPt 6:1, yet has a higher total surface area (for all other samples a higher diameter meant lower surface area). Total surface area is not the only factor in catalytic activity, but its effect is indeed significant. Further examinations of the effects of the total surface area are in the following section.

3.2 PEM Fuel Cell Application

After applying the nanoparticles to Nafion membranes, we tested Au, Ag, AuAg, PtAg, AuPt, AuPt 6:1, and the control membranes at the PEMFC testing station. Highest recorded power output from each membrane, when compared to the output of the control membrane, is shown in Figure 9.

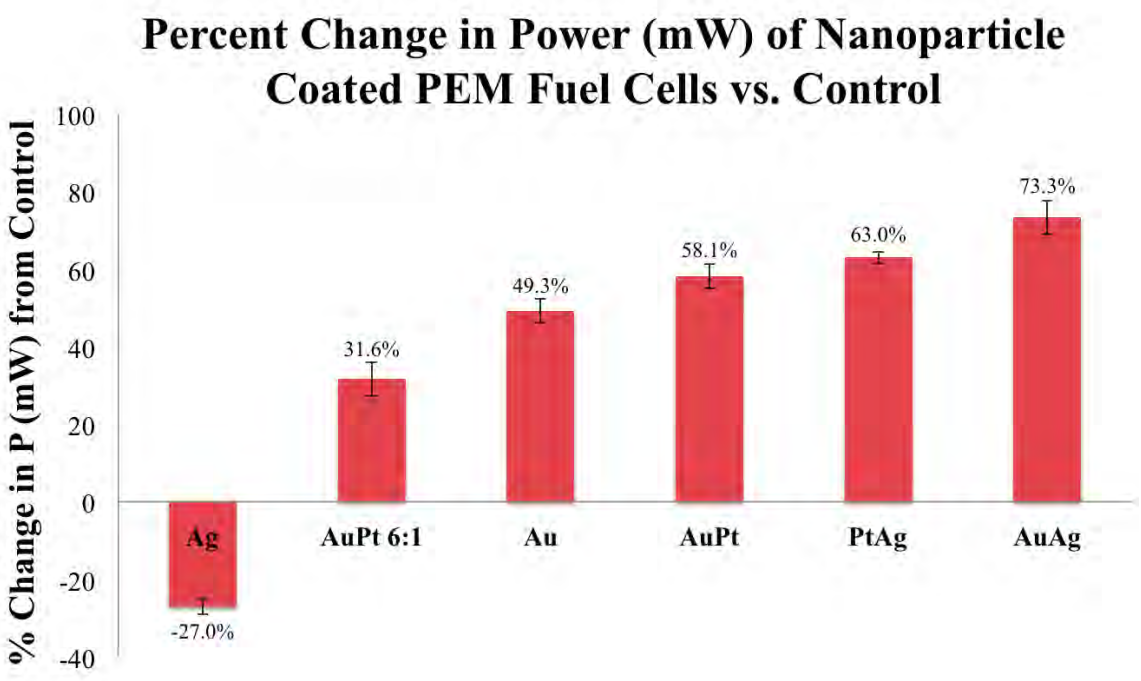

Figure 9: Comparisons of the maximum power output of each type of PEMFC with the control, listed in increasing percentage increases in power output. Data labels above each bar show the percentage increase in power output compared to the control.

Power output is an important measure of the efficiency of a fuel cell. All PEM fuel cells received the same rate of hydrogen gas flow, but some coatings converted the gas into power more effectively than did others. Using the uncoated control membrane as a baseline, the bimetallic AuAg coating had the greatest power increase of 73.3% from 175 mW to 304 mW. AuAg surpassed the performance of all other coatings in power output, including even AuPt, which had a power increase of 58.1% from the control, despite AuPt having been reported to be the best performance-enhancement coating.[3] In fact, even the PtAg membrane at a power increase of 63.0% performed better than AuPt. Both AuAg and PtAg contained silver, an ingredient that was not expected to work well in fuel cells (which is true when silver is in its pure form).

A wide range of resistance values is necessary when testing the practicality of a coating in fuel cells. Figure 10 plots the results for all tested additional resistances, with 0 Ω of additional resistance resulting in the highest power and current and ∞ Ω of added resistance causing the

lowest power and current. Note that we are not short-circuiting the system at 0 Ω of additional resistance–there is still internal resistance of the circuit.

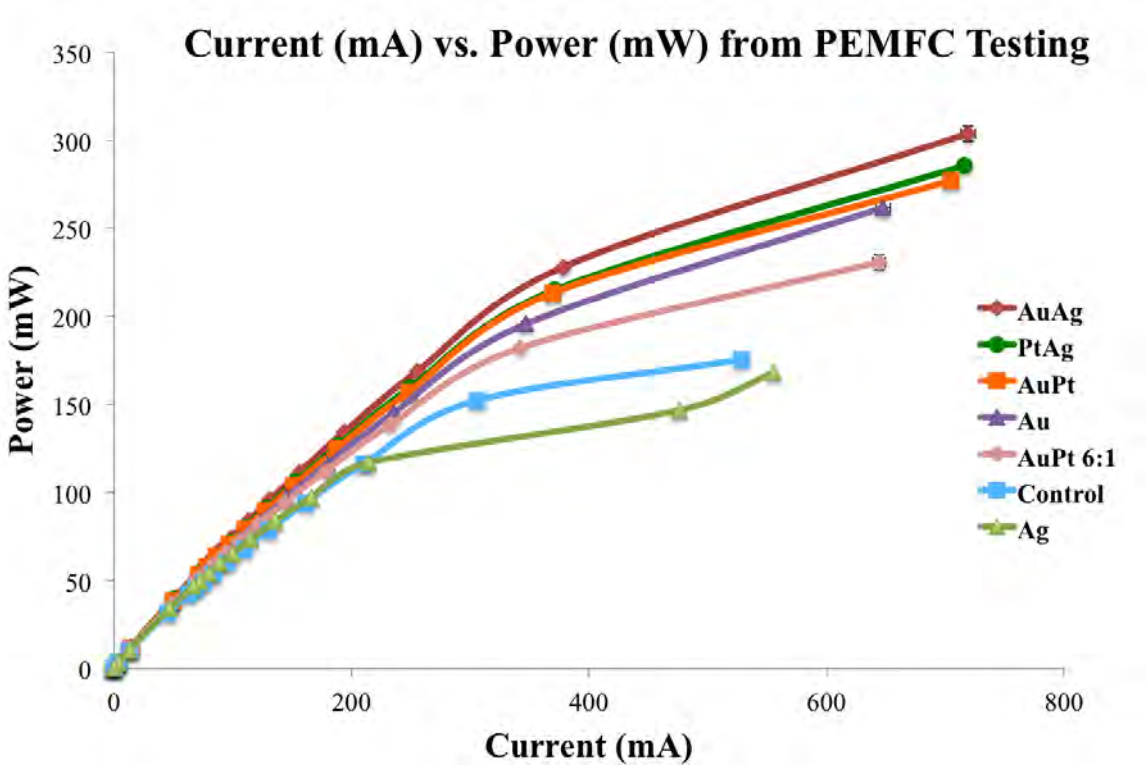

Figure 10: Power vs. current data gathered from our PEMFC testing. We altered the amount of additional resistance in order to create varying values of current and voltage (and therefore, power).

Generally, current and power both increase as resistance decreases. Current and power for the samples at high resistance overlap near the origin where the current is less than 200 mA, whereas results towards smaller resistances (greater currents) vary greatly. Ag nanoparticles performed worse than the control membrane at low resistance values, while AuAg exhibited superior current and power output across the board.

The AuAg coating was the best at splitting H_2 into $2\,H^+$ and $2\,e^-$ while preventing CO poisoning. The reasons to be explained for the improvement in performance involve size, surface area, distribution, and stability, together with noble metal identities, properties, and interactions.

In the same volume, smaller particles generally imply greater surface area, which increases the number of binding sites for catalysis, and therefore increases the catalytic activity of the

material. AuAg (mean size of 4.2 ± 0.6 nm) was smaller than both of its component metals (Au and Ag), allowing greater access to H_2 interactions. However, the mean size of AuAg was greater than AuPt 6:1, AuPt 1:6, PtAg, and AuPt, all of which performed worse than AuAg. Analysis of total surface area with equation 3 revealed that only AuPt and PtAg had a higher total surface area than AuAg. AuAg had a low density, increasing the total surface further above AuPt 6:1 and AuPt 1:6 despite its larger size. This unusually high total surface area for AuAg greatly increased its catalytic activity. In a new computational paper, researchers found a decrease in catalytic performance in platinum particles from 1 nm to 3 nm due to excessively strong binding forces to the reactants, making them difficult to detach and catalytically inactive.[21] PtAg and AuPt both had a mean diameter less than 3 nm, so their performance might be affected negatively by this effect. Although the samples were not pure platinum, the platinum component in each sample was most likely affected by this size-activity limitation. In addition, the electrodes already contained platinum coatings, making the marginal enhancements from adding more platinum nanoparticles in the Nafion membrane increasingly negligible compared to the effect of adding other metals such as gold and silver.

Nanoparticle shape and distribution factored into catalytic activity. AuAg nanoparticles were evenly distributed, small, spherical particles, creating many openings for hydrogen gas to penetrate and attach to the binding site of the catalyst. In addition, the stability of AuAg with a Zeta Potential of -84.66 mV meant not only longevity in suspension but also a greater control over reactions, even in membranes. The pure Ag nanoparticles' unusually large size and low total surface area combined with their instability (easily oxidizable nature of pure silver) caused the catalytic activity to decrease. The large particle size and oxidized silver obstructed the PEM and prevented catalysis.

PtAg and AuPt coatings were both less effective than AuAg at increasing power output. The innate properties and interactions behind these bimetallic nanoparticles may explain this. Silver is significantly more reactive and less stable than gold,[8] so having a component of silver in the AuAg alloy would provide the benefit of having more free electrons to be used in catalysis, but we expected a decrease in stability. Gold's closed-shell nature makes it less reactive than

silver and therefore less efficient in splitting H_2, but resistance to oxidation and catalysis of $CO \longrightarrow CO_2$ protected the system (especially the Pt catalyst in the carbon paper) from CO poisoning and oxidation, thus increasing both efficiency and stability.[8] PtAg still gained the increased reactivity from silver, but was vulnerable to poisoning as platinum only offered catalytic enhancement and not protection. AuPt had protection from CO poisoning, but a lack of significant increase in reactivity led to lower catalytic activity than the silver alloy nanoparticles. The pumping of electrons by silver and poisoning/oxidation protection by gold combined to produce the ideal alloy for $H_2 \longrightarrow 2\,H^+ + 2\,e^-$ catalysis, CO resistance, and oxidation resistance.

4 Conclusion and Future Work

4.1 Conclusion

We synthesized 10 different types of noble metal alloy nanoparticles using a two-phase modified Brust-Schiffrin method, characterized them using ultraviolet-visible spectroscopy, zeta potential, and transmission electron microscopy, and applied them to a Nafion 117 membrane to test for catalytic activity.[2] We synthesized particles in the 2 nm - 6 nm range (with the exception of pure silver), found that AuAg was the most stable of our particles according to its large zeta potential value – and therefore the most practical for large-scale use – and achieved a 73% increase in PEM fuel cell power output using AuAg-coated Nafion membranes when compared to the control membrane. By using only 200 μL of our nanoparticle suspension to coat a Nafion membrane, we have increased the power output per dollar of PEMFC: the benefits of the 73% power increase certainly outweigh the costs of applying the coating. Our research identifies a pathway that is quite promising: there is ample room for improvement in the PEMFC field, and testing different alloys is one approach to achieve this improvement. PEMFC using noble metal alloys such as AuAg demonstrate a clean and green alternative energy source, and can be manufactured in a cost-effective manner.

4.2 Future Work

Since we expected the greatest enhancement in catalytic activity to come from the AuPt alloys as shown in literature,[3] we varied ratios for only AuPt alloys – which surprisingly turned out to be less effective catalysts than our other alloys – and did not attempt to make different ratios of other metals. An important step in enhancing the fuel cell efficiency even further would be to vary the ratios of AuAg and PtAg and run the same PEMFC tests after coating Nafion membranes with the particles. A significant and practical finding from our research was that the optimal combination of noble metals (AuAg) did not include platinum, the most expensive of the three metals. If implemented, this would make the manufacturing process more economical. Metals we did not have the opportunity to test, such as cobalt, palladium, copper, and ruthenium, should be tested for use in alloys. A combination of three metals in one alloy, a ternary alloy, could yield interesting results in characterization, notably in the UV-Visible spectroscopy (as shown in Figure 4) and power output. We could study the morphology of the Nafion membrane impregnated with the nanoparticles to find the reason for AuAg's significant power increase. Furthermore, as a way to optimize the systems, we could study the reactions at the anode and cathode and replace the Pt in the existing electrode layer with an alloy such as AuAg. Experimentation with different capping agents could be performed to control the sizes of the nanoparticles to around 3.1 nm, which would theoretically maximize their catalytic activity according to computational models.[21]

For applications to transportation vehicles or industrial settings, increasing membrane size or stacking multiple fuel cells together would be necessary to achieve the desired power output. It would be difficult to increase membrane size for testing in our current laboratory setting, but linking multiple cells or testing in a larger laboratory is a reasonable endeavor.

Our work is not limited to PEM fuel cells; the potential applications of nanoparticles are many, and our alloy testing approach could be applied to electrolyzers, flow cells, electronics manufacturing, laser generation, and a wide range of other fields in attempts to enhance performance.

5 Acknowledgements

For Mentoring, Stony Brook University Department of Materials Science and Engineering

Tatsiana Mironava

Hongfei Li

Miriam Rafailovich

For Proofreading, Staples High School

AJ Scheetz

Humphrey Wong

Karen Thompson

Michele Morse

Nicholas Morgan

William Jones

Ulyana Piterbarg

Rees Chang

6 References

[1] Stark, W. J., Stoessel, P. R., Wohllebenb, W. and Hafnerc, A. (2015). Industrial applications of nanoparticles. *Chem. Soc. Rev.*, 2015, 44, 5793-5805.

[2] Brust, M., Walker, M., Bethell, D., Schiffrin, D., & Whyman, R. (1994). Synthesis of thiol-derivatised gold nanoparticles in a two-phase Liquid-Liquid system. *Journal of the Chemical Society, Chemical Communications J. Chem. Soc., Chem. Commun.,* 801-801.

[3] Fang, B., Wanjala, B., Xiang, H., et. al. (2011). Proton exchange membrane fuel cells with nanoengineered AuPt catalysts at the cathode. *Journ. Power Sources.*, 2011

[4] Nafion 117 perfluorinated membrane. 274674 ALDRICH. *Sigma-Aldrich*

[5] Pacala, S. (2004). Stabilization Wedges: Solving the Climate Problem for the Next 50 Years with Current Technologies. *Science*, 968-972.

[6] Sasaki, K., Naohara, H., Cai, Y., Choi, Y., Liu, P., Vukmirovic, M., & Adzic, R. (2010). Core-Protected Platinum Monolayer Shell High-Stability Electrocatalysts for Fuel-Cell Cathodes. *Angewandte Chemie*, 8784-8789.

[7] Landman, U., Yoon, B., Zhang, C., Heiz, U., & Arenz, M. (2007). Factors in Gold Nanocatalysis: Oxidation of CO in the Non-Scalable Size Regime. *ChemInform.*

[8] Jamshidi, Z., Eskandari, K., & Azami, S. (2013). Nature of closed- and open-shell interactions between noble metals and rare gas atoms. *Int. J. Quantum Chem. International Journal of Quantum Chemistry*, 1981-1991.

[9] Haruta, M. (2004). Nanoparticulate Gold Catalysts for Low-Temperature CO Oxidation. *ChemInform.*

[10] Green, I., Tang, W., Neurock, M., & Yates, J. (2014). ChemInform Abstract: Insights into Catalytic Oxidation at the Au/TiO2 Dual Perimeter Sites. *ChemInform.*

[11] Green, I., Tang, W., Neurock, M., & Yates, J. (2011). Spectroscopic Observation of Dual Catalytic Sites During Oxidation of CO on a Au/TiO2 Catalyst. *Science*, 736-739.

[12] Green, I., Tang, W., Neurock, M., & Yates, J. (2011). Low-Temperature Catalytic H2 Oxidation over Au Nanoparticle/TiO2 Dual Perimeter Sites. *Angewandte Chemie Angew. Chem.,* 10368-10371.

[13] Dunbar, Brian. "Liquid Hydrogen–the Fuel of Choice for Space Exploration." *NASA.* NASA, 29 July 2010. Web. 9 Sept. 2015.

[14] "A Basic Overview of Fuel Cell Technology." *A Basic Overview of Fuel Cell Technol-*

ogy. American History. Web. 1 Sept. 2015.

[15] Sigma-Aldrich. 2014. Proton Electron Membrane Figure 2. Retrieved from sigmaaldrich.com/content/d aldrich/materials-science/alternative-energy/pem-fuel-cells/figure-2.gif

[16] Greenwood, R; Kendall, K (1999). "Electroacoustic studies of moderately concentrated colloidal suspensions." *Journal of the European Ceramic Society* 19 (4): 479-488.

[17] KSV NIMA Langmuir and Langmuir-Blodgett Deposition Troughs. (2014).

[18] "Gold Nanoparticles: Properties and Applications." *Sigma-Aldrich.* 2012. Web. 11 Oct. 2015.

[19] Bhui, D., Bar, H., Sarkar, P., Sahoo, G., De, S., & Misra, A. (2009). Synthesis and UV-vis spectroscopic study of silver nanoparticles in aqueous SDS solution. *Journal of Molecular Liquids*, 33-37.

[20] Dunleavy, J. (2006). Final Analysis: Sulfur as a Catalyst Poison. *Platinum Metals Review*, 110-110.

[21] Tan, T., Wang, L., Zhang, J., Johnson, D., & Bai, K. (2015). Platinum Nanoparticle During Electrochemical Hydrogen Evolution: Adsorbate Distribution, Active Reaction Species, and Size Effect. *ACS Catalysis*, 2376-2383.